



Extreme wave run-up on a vertical cliff

Francesco Carbone, Denys Dutykh, John M. Dudley, Frédéric Dias

► To cite this version:

Francesco Carbone, Denys Dutykh, John M. Dudley, Frédéric Dias. Extreme wave run-up on a vertical cliff. *Geophysical Research Letters*, 2013, 40 (12), pp.3138-3143. 10.1002/grl.50637 . hal-00799118v3

HAL Id: hal-00799118

<https://hal.science/hal-00799118v3>

Submitted on 31 May 2013

HAL is a multi-disciplinary open access archive for the deposit and dissemination of scientific research documents, whether they are published or not. The documents may come from teaching and research institutions in France or abroad, or from public or private research centers.

L'archive ouverte pluridisciplinaire **HAL**, est destinée au dépôt et à la diffusion de documents scientifiques de niveau recherche, publiés ou non, émanant des établissements d'enseignement et de recherche français ou étrangers, des laboratoires publics ou privés.

EXTREME WAVE RUN-UP ON A VERTICAL CLIFF

FRANCESCO CARBONE, DENYS DUTYKH*, JOHN M. DUDLEY, AND FRÉDÉRIC DIAS

ABSTRACT. Wave impact and run-up onto vertical obstacles are among the most important phenomena which must be taken into account in the design of coastal structures. From linear wave theory, we know that the wave amplitude on a vertical wall is twice the incident wave amplitude with weakly nonlinear theories bringing small corrections to this result. In this present study, however, we show that certain simple wave groups may produce much higher run-ups than previously predicted, with particular incident wave frequencies resulting in run up heights exceeding the initial wave amplitude by a factor of 5, suggesting that the notion of the design wave used in coastal structure design may need to be revisited. The results presented in this study can be considered as a note of caution for practitioners, on one side, and as a challenging novel material for theoreticians who work in the field of extreme wave - coastal structure interaction.

Key words and phrases: run-up; wave/wall interaction; Serre equations; coastal structures; wave groups

CONTENTS

1	Introduction	1
2	Numerical study	4
2.1	Numerical scheme and set-up	4
2.2	Numerical results	5
3	Conclusions and perspectives	10
	Acknowledgments	10
	References	11

1. Introduction

The robust design of various coastal structures (such as sea-walls, breakwaters, etc.) relies on the accurate estimation of the wave loading forces. To this end, engineers have introduced the notion of the so-called *design wave*. Once the particular characteristics of this design wave are determined, the pressure field inside the bulk of fluid is usually reconstructed (in the engineering practice) using the [32] or [17] semi-empirical formulas. However, there is a difficulty in determining the wave height to be used in design works. Sometimes, it is taken as the significant wave height $H_{1/3}$, but in other cases it is $H_{1/10}$ (the

* Corresponding author.

average of 10% highest waves) that are substituted into the wave pressure formulas. If we take, for example, an idealized sea state which consists only of a single monochromatic wave component with amplitude a_0 , its wave height H_0 can be trivially computed

$$H_0 \equiv H_{1/3} \equiv H_{1/10} = 2a_0. \quad (1.1)$$

Consequently, the design wave will have also the height equal to $2a_0$.

In the present study, we show that even such simple monochromatic sea states, subject to the nonlinear dynamics over a constant bottom, can produce much higher amplitudes on a vertical wall. Namely, we show below that some wave frequencies can lead to an extreme run-up of the order of $\approx 5.5a_0$ on the cliff. The results presented in this study suggest that the notion of the design wave has to be revisited. Moreover, the mechanism elucidated in this work can shed some light onto the freak wave phenomenon in the shallow water regime, where we recall in this context that over 80% of reported past freak wave events have been in shallow waters or coastal areas [29, 30].

It is well known that wave propagation on the free surface of an incompressible homogeneous inviscid fluid is described by the Euler equations combined with nonlinear boundary conditions on the free surface [38]. However, this problem is difficult to solve over large domains and, consequently, simplified models are often used. In particular, in this study we focus our attention on long wave propagation. A complete description of wave processes, including collisions and reflections, is achieved by employing two-way propagation models of Boussinesq type [2]. Taking into account the fact that we are interested here in modeling (potentially) high amplitude waves, we adopt the fully nonlinear Serre–Green–Naghdi (SGN) equations [35, 18, 19, 44], which make no restriction on the wave amplitude. Only the weak dispersion assumption is adopted in the mathematical derivations of this model [41, 23, 12].

We consider a two-dimensional wave tank with a flat impermeable bottom of uniform depth $d = \text{const}$, filled with an incompressible, inviscid fluid (see Figure 1). The Cartesian coordinate system Oxy is chosen such that the y -axis points vertically upwards and the horizontal x -axis coincides with the undisturbed water level $y = 0$. The free surface elevation with respect to the still water level is denoted by $y = \eta(x, t)$ and hence, the total water depth is given by $h(x, t) = d + \eta(x, t)$. Denoting the depth-averaged horizontal velocity by $u(x, t)$, the SGN system reads [23, 12, 8]:

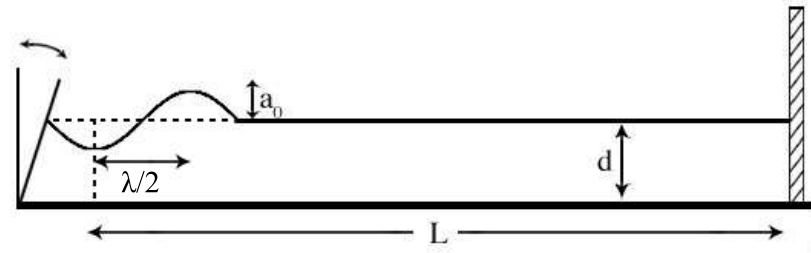
$$h_t + (hu)_x = 0, \quad (1.2)$$

$$u_t + \left(\frac{1}{2}u^2 + gh\right)_x = \frac{1}{3}h^{-1} \left[h^3(u_{xt} + uu_{xx} - u_x^2) \right]_x, \quad (1.3)$$

where g is the acceleration due to gravity.

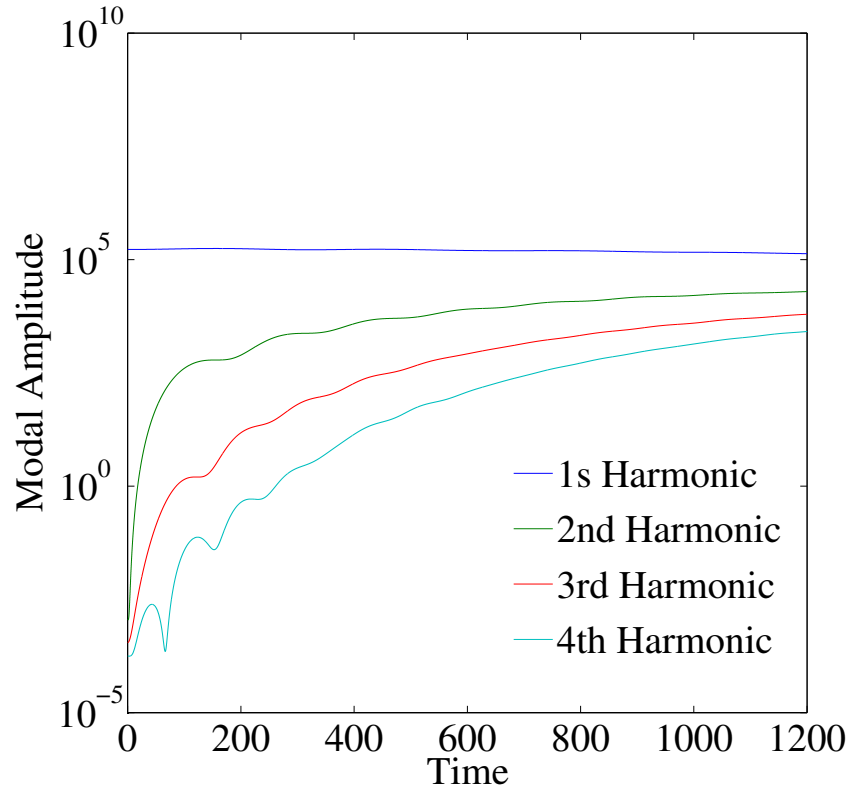
The SGN system possesses Hamiltonian and Lagrangian structures [24, 8] and conservation laws for mass, momentum, potential vorticity and energy [24, 14]. From a more physical perspective the SGN model combines strong nonlinear effects with some dispersion that approximates well the full water wave dynamics. This model has been previously validated by extensive comparisons with experimental data for wave propagation and run-up [7, 40, 5, 14].

One of the most important questions in water wave theory is the understanding of wave interactions and reflections [25, 1, 9] and the interaction of solitary waves has also been



(a)

$$\omega = 0.01$$



(b)

Figure 1. Upper panel (a): schematic view of the numerical experiments. Here L is the length of the computational domain, d is the uniform water depth, a_0 is the incoming wave amplitude and λ is its wavelength; lower panel (b): temporal evolution of the first four harmonics of a sinusoidal wave of frequency $\omega = 0.01$ injected in the domain (in the absence of the right wall).

extensively studied [43, 3, 16, 11]. By using symmetry arguments, one can show that the head-on collision of two equal solitary waves is equivalent to the solitary wave/wall interaction in the absence of viscous effects.

The accurate determination of the maximum wave height on a wall is of primary importance for applications. Several analytical predictions for periodic or solitary wave run-up \mathcal{R}_{\max} in terms of the dimensionless wave amplitude $\alpha = a_0/d$ have been developed: linear theory [27] $\mathcal{R}_{\max}/d = 2\alpha$; third-order theory [39] $\mathcal{R}_{\max}/d = 2\alpha + 1/2\alpha^2 + 3/4\alpha^3$, and nonlinear shallow water theory [28] $\mathcal{R}_{\max}/d = 4(1 + \alpha - \sqrt{1 + \alpha}) = 2\alpha + 1/2\alpha^2 - 1/4\alpha^3 + \mathcal{O}(\alpha^4)$.

These results have been confirmed in previous experimental [26], theoretical [4] and numerical [16, 11] studies. All these theories agree on the fact that the wave height on the wall is two times the incident wave amplitude plus higher order corrections. This conclusion provides a theoretical justification for the use of a wave height such as $H_{1/3}$ in the design wave definition.

2. Numerical study

From a practical point of view, however, the reasoning presented above contains at least one serious flaw — in real-world conditions, waves seldom come isolated but rather as groups. In this Section, we show numerically how simple wave groups can produce much higher run-ups than expected from the existing theoretical predictions.

Our numerical wave periods cover a range between 20 s and 1100 s (i.e. for $6 < d < 30$ m and $g = 9.81$ m/s²), from long swells to tsunami waves. Extreme run-ups are obtained for wave periods which are in between swell periods and tsunamis periods, corresponding possibly to tsunamis generated by underwater landslides. Moreover, we take as initial conditions waves which are not exact solutions to the equations. Naturally they deform as they evolve towards the vertical wall. This deformation is reminiscent of the transformation of waves over sloping bathymetries.

2.1. Numerical scheme and set-up

Let us consider a flat channel of constant depth d and length L . This channel is bounded on the right by a rigid vertical wall and by a wavemaker on the left (see Figure 1). We use dimensionless variables where lengths are normalized with d , speeds with \sqrt{gd} and time with $\sqrt{d/g}$. This scaling is equivalent to setting $g = 1$ m/s², $d = 1$ m in the governing equations (1.2) and (1.3).

In order to solve numerically the SGN equations we use the high-order finite-volume scheme described in [14]. This scheme has been successfully validated against analytical solutions and experimental data [20]. For the time integration we use the classical fourth-order Runge–Kutta scheme [36, 37]. The computational domain is divided into equal intervals (i.e. control volumes) such that we have $N = 1000$ control volumes per wavelength. The convergence study showed that this grid provides a good trade-off between accuracy and overall computational time. Note that the extreme run-up values reported in this study can slightly increase under mesh refinement, which decreases the effect of numerical dissipation. All simulations start with the rest state $\eta(x, t = 0) \equiv 0$, $u(x, t = 0) \equiv 0$.

The wavemaker generates a monochromatic incident wave:

$$\eta(x = 0, t) = \eta_0(t) = a_0 \sin(\omega t) \mathcal{H}(T - t), \quad (2.1)$$

where the amplitude $a_0 = 0.05$, $\omega \in [0.01, 0.25]$ and $\mathcal{H}(t)$ is the Heaviside function and c_s is the wave speed $c_s = \sqrt{g(d + a_0)}$ [14]. An important remark should be made on the initialization of the problem: sometimes spurious high-frequency standing waves are generated when numerical simulations of nonlinear progressive waves are initialized using linear waves (in particular for deep water waves). In such cases the problem should be initialized by suppressing the spurious generation of standing waves. However, a nonlinear simulation can be initialized with simple linear waves if the runtime is long enough to adjust the wave shape [13]. As can be seen in the lower panel of Figure 1 the amplitude of the first harmonic remains constant during the propagation while the amplitudes of the higher harmonics tend to increase until a constant value is reached, as illustrated in [13]. For this reason no adjustment is required in our case.

We generate only a finite number N_w of waves with period $T_0 = 2\pi/\omega$ and thus, the wave generation time T is defined as $T = N_w T_0$. The monochromatic deviation of the free surface at the left boundary is then propagated towards the right wall under the SGN dynamics. The length L of the computational domain and the final simulation time T_f are chosen adaptively in order to allow all important interactions and to prevent any kind of reflections with the left generating boundary:

$$L = (N_w + \frac{1}{2})\lambda, \quad T_f = \frac{L}{\sqrt{g(d + a_0)}} + T,$$

λ being the wavelength corresponding to the frequency ω .

2.2. Numerical results

We begin our numerical experiments by considering a single sinusoidal wave interacting with the solid wall. In Figure 2 we show three snapshots of the single wave evolution at three different times, i. e. before reaching the wall, during the impact and right after the reflection. The initial sinusoidal wave undergoes steepening during its propagation. The run-up on the vertical wall is shown on the lower panel of Figure 2. The maximal dimensionless wave elevation $\mathcal{R}_{\max} \simeq 0.10245$ on the wall reaches roughly twice the incident wave amplitude $a_0 = 0.05$ (at $t \simeq 70$). This result is in good agreement with previous numerical studies on the solitary waves interactions [10, 31, 6] even if the incident shape is not exactly the same. The maximal relative run-up $\mathcal{R}_{\max}/a_0 \simeq 2.34$ is achieved for $\omega_{\max} = 0.145$. The value of \mathcal{R}_{\max} is slowly decreasing for $\omega > \omega_{\max}$.

When two waves are injected into the domain, the dynamics is similar to the single wave case. However, with two waves the nonlinear effects become even more apparent (see Figure 3).

In a certain range of wave periods ($\omega \in (0.01, 0.05)$), the so-called *dispersive shock waves* are formed [41, 40]. This particular type of solution has been extensively studied theoretically and numerically in [15]. When the second wave impinges on the first reflected wave, a dispersive shock wave forms and propagates towards the wall. As shown in the last panel of Figure 3 the maximal amplification is achieved when the second wave hits the wall due to nonlinear interactions between two counter-propagating waves. However, we underline that with only two waves one can achieve a maximal run-up on the wall \mathcal{R}_{\max} of

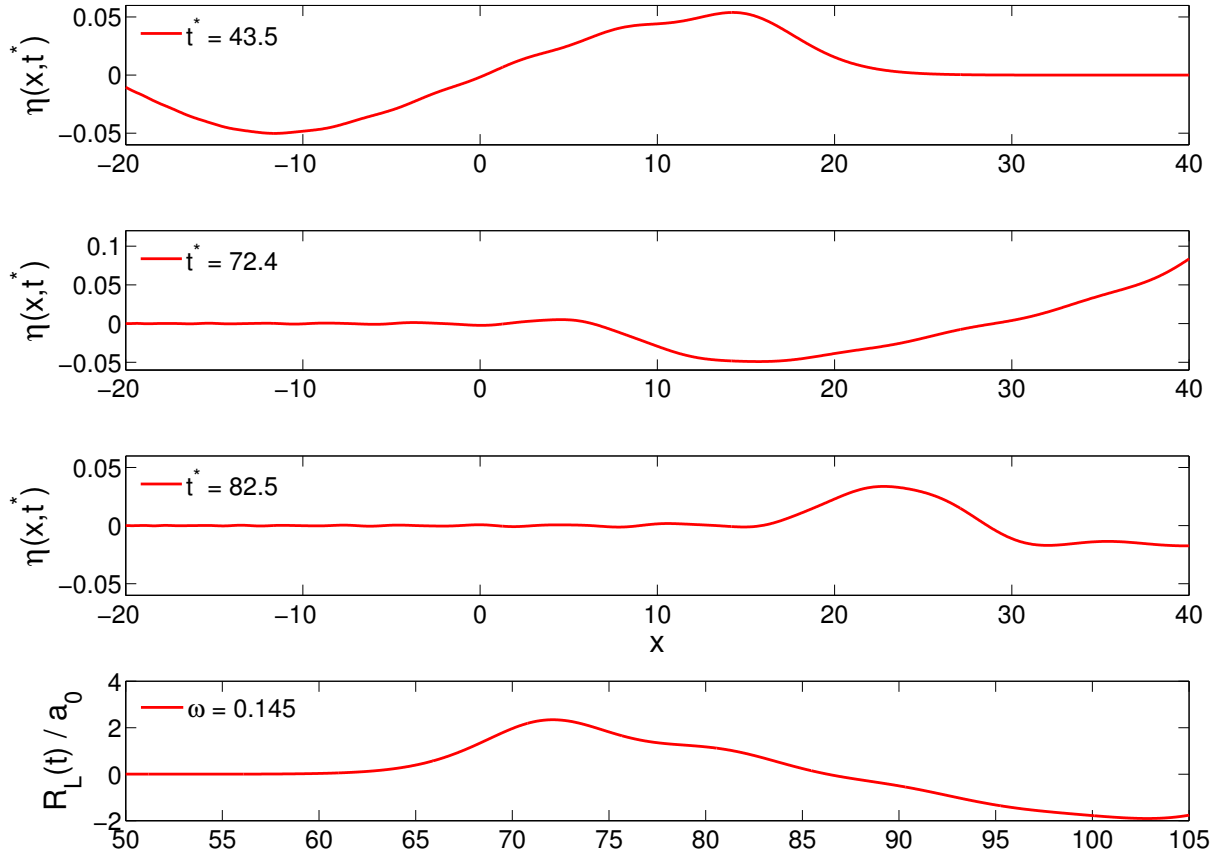


Figure 2. Time evolution of the free surface elevation as a function of space, at three different times t^* (first three top panels) reported on the figure. The figure refers to the single-wave case with frequency $\omega = 0.145$. The lower panel reports the maximal elevation at the wall \mathcal{R}_L/a_0 as a function of time.

almost four incident wave amplitudes a_0 :

$$\mathcal{R}_{\max}/a_0 \simeq 3.8, \quad \text{for} \quad \omega = 0.021. \quad (2.2)$$

Such high run-up values are possible due to the energy transfer between the first reflected wave and the second incoming wave. The dependence of the maximal run-up \mathcal{R}_{\max} on the incident wave frequency ω and the number N_w of incident waves is shown in Figure 4. One can see from this figure that the optimal energy transfer due to dispersive shocks happens for three incident waves (see Figure 6). In this case the maximal run-up is observed around $\omega_{\max} = 0.035$ and the amplification is equal to $\mathcal{R}_{\max}/a_0 \simeq 5.43$. However, the energy transfer process is saturated for three waves.

We performed similar computations with four incident waves (also shown on Figure 4) and the maximal run-up is not higher than with three waves. Consequently, we focus now only on the *optimal* three-wave case. The three regimes (hyperbolic, equilibrium and dispersive) are illustrated on Figure 7, where we show the space-time dynamics of the three-wave system. The left panel shows the hyperbolic regime. On the central panel strong

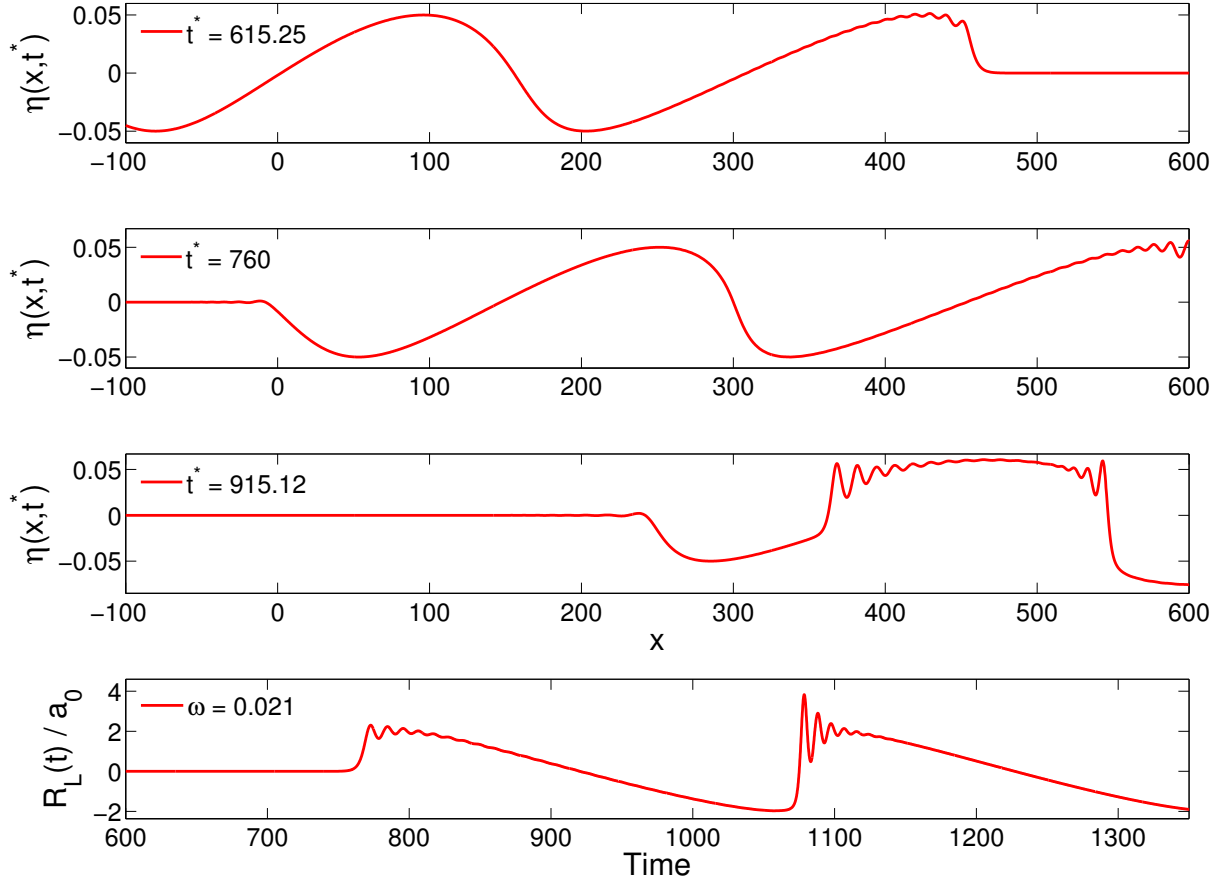


Figure 3. Time evolution of the free surface elevation as a function of space, at three different times t^* (first three top panels) reported on the figure. The figure refers to the two-wave case with frequency $\omega = 0.021$. The lower panel reports the maximal elevation at the wall R_L/a_0 as a function of time.

dispersive shocks can be observed, while on the right panel the dynamics is smoothed by the dispersion. In the last case the amplification is mainly produced by the linear superposition of the incident and reflected waves. The reflection and interaction are clearly observed by smooth secondary peaks in the space time plots (see Figure 7, but also Figure 5).

The wave interactions described above strongly depend on the frequency ω of the impinging waves as can be seen in Figure 5, where we show the wave records on the wall for several values of the frequency ω . As the wave frequency increases, the wavelength shortens and the dispersive effects become gradually more important. Around ω_{\max} the dispersive effects are balanced with nonlinearities to produce the most pronounced dispersive shock waves. Starting from $\omega \simeq 0.11$ we enter into the dispersive regimes where the waves become regularized.

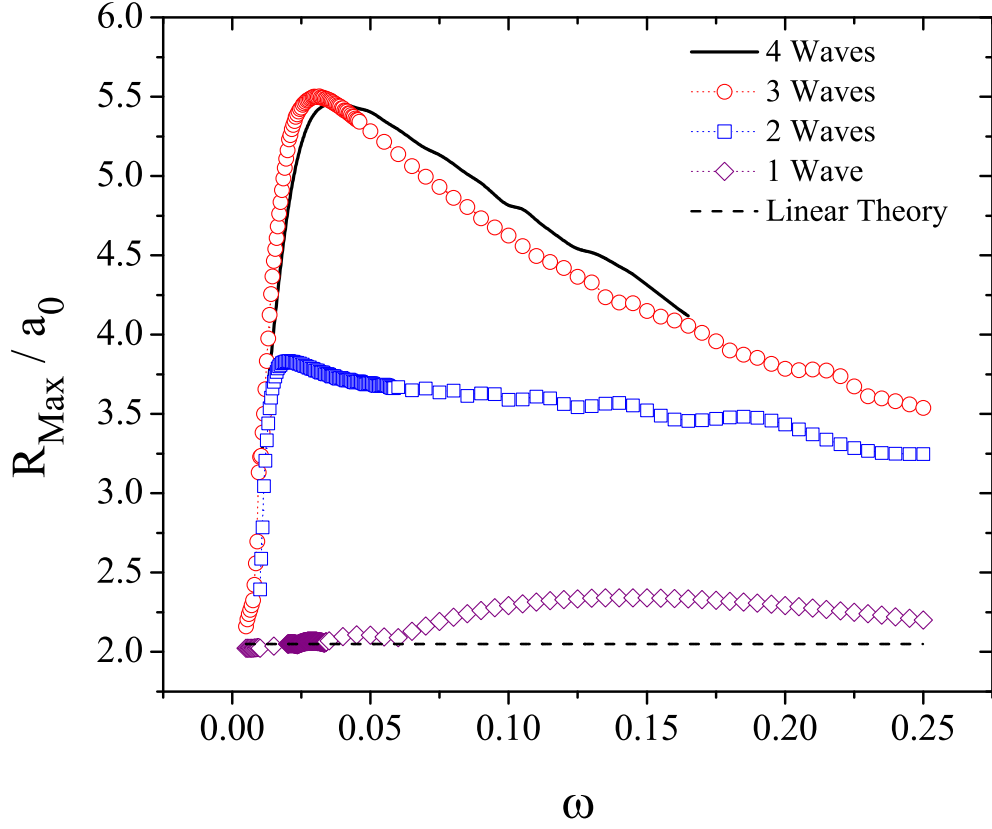


Figure 4. Maximum wave run-up \mathcal{R}_{\max}/a_0 on the right vertical wall as a function of incoming wave frequency for different numbers of incident pulses: 1 (squares), 2 (circles), 3 (triangles) and 4 (solid line). The dashed line represents the linear limit where $\mathcal{R}_{\max}/a_0 \equiv 2$.

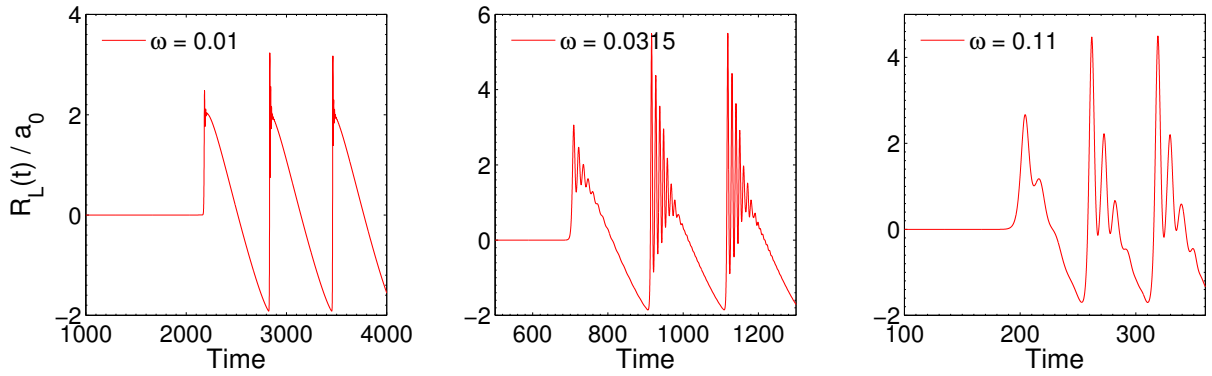


Figure 5. Time evolution of the wave run-up on the vertical wall for the three incident wave case recorded for several values of the incoming frequency ω . The maximum run-up is achieved for $\omega_{\max} \approx 0.0315$.

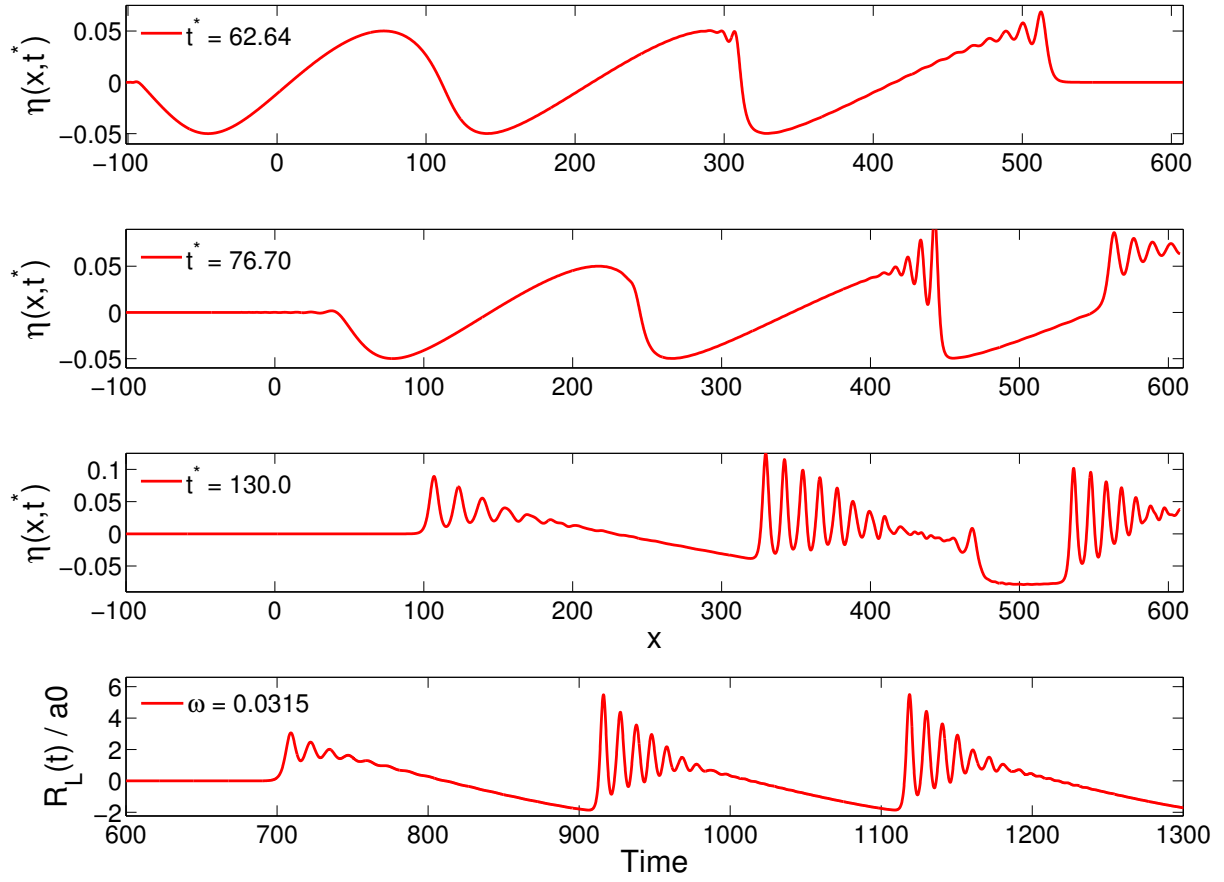


Figure 6. Time evolution of the free surface elevation as a function of space, at three different times t^* (first three top panels) reported on the figure. The figure refers to the three-wave case with frequency $\omega = 0.0315$. The lower panel reports the maximal elevation at the wall \mathcal{R}_L/a_0 as a function of time.

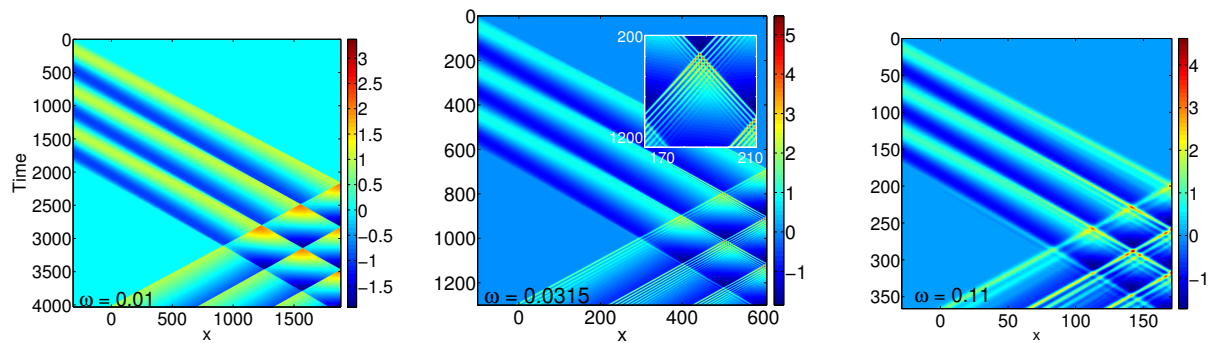


Figure 7. Space-time evolution plots for the three incident wave case shown for three particular values of the wave frequency ω .

3. Conclusions and perspectives

In the present study we investigated numerically the interaction between a wave and a vertical wall in the framework of the Serre–Green–Naghdi (SGN) equations. These equations combine strong nonlinear and weak dispersive effects. We explored the whole range of wavelengths from the hyperbolic regime (including shock waves) to smooth dispersive waves ($\omega \gtrsim 0.1$). More importantly, we showed that the wave run-up on the wall is strongly dependent on the incident wave frequency, the dependence not being monotonic. In particular, there is a fixed frequency ω_{\max} which provides the maximum long wave run-up on the vertical wall. The function $\mathcal{R}_{\max}(\omega)$ is monotonically increasing up to ω_{\max} and monotonically decreasing for $\omega > \omega_{\max}$ (at least within the range of considered numerical parameters). The dynamics can be conventionally divided into three main stages:

- (1) Propagation of the wave group towards the wall along with the front steepening and other nonlinear deformations
- (2) First wave run-up and its reflection from the wall
- (3) Projection of the reflected energy again onto the wall by subsequent incident waves

The maximal observed amplification $\approx 5.5a_0$ is achieved with only three incident waves. For example, on a 10 m water depth the *critical* period is equal approximatively to $T_{\max} \approx 180$ s ($\omega_{\max} \equiv 2\pi/T_{\max}$). Such a wave period can be generated by small underwater landslides.

The results presented in this study shed light onto extreme wave run-ups on vertical cliffs and similar coastal structures. Moreover, in view of these results, the definition of the *design wave* has to be revisited. Our suggestion would be to take at least $3H_{1/3}$ or even $3H_{1/10}$. The present results also shed some new light on the mysterious accumulations of large boulders on cliff tops up to 50 m high on the deep water coasts, especially on the west coast of Ireland [21, 42, 30]. The emplacement of these megaclasts is usually attributed to extreme storm waves, but there are also those who believe that tsunamis are the most probable explanation of boulder ridges in these areas [22, 34, 33].

In future investigations, more general wave groups have to be studied to unveil their potential for focussing on the walls. We recall that so far we considered only simple idealized monochromatic waves. In addition, we are going to investigate the effect of the forces exerted by incident waves on vertical obstacles, which can be different from the purely kinematic amplitude focussing presented in this study. In other words, it is not clear whether the highest wave will produce the highest dynamic pressure spike on the wall. The effect of the wave amplitude is to be investigated as well since all the processes under consideration are highly nonlinear. Some theoretical explanation of these phenomena is also desirable. However, the difficulty is rather high again because of important nonlinearities mentioned hereinabove. We claim that no linear theory is sufficient to provide a satisfactory explanation.

Acknowledgments

This work was funded by ERC under the research project ERC-2011-AdG 290562-MULTIWAVE and SFI under Grant Number SFI/12/ERC/E2227. The authors wish to

acknowledge the SFI/HEA Irish Centre for High-End Computing (ICHEC) for the provision of computational facilities and support under the project “*Numerical simulation of the extreme wave run-up on vertical barriers in coastal areas*”. We would like also to thank Alizée DUBOIS who obtained the first preliminary results on this subject during her visit to University College Dublin in May 2012.

References

- [1] K. M. Berger and P. A. Milewski. Simulation of wave interactions and turbulence in one-dimensional water waves. *SIAM Journal on Applied Mathematics*, 63(4):1121–1140, 2003. [2](#)
- [2] J. L. Bona and M. Chen. A Boussinesq system for two-way propagation of nonlinear dispersive waves. *Physica D*, 116:191–224, 1998. [2](#)
- [3] J. L. Bona, W. G. Pritchard, and L. R. Scott. Solitary-wave interaction. *Phys. Fluids*, 23:438–441, 1980. [3](#)
- [4] J. G. B. Byatt-Smith. The reflection of a solitary wave by a vertical wall. *J. Fluid Mech.*, 197:503–521, 1988. [4](#)
- [5] J. D. Carter and R. Cienfuegos. The kinematics and stability of solitary and cnoidal wave solutions of the Serre equations. *Eur. J. Mech. B/Fluids*, 30:259–268, 2011. [2](#)
- [6] J. Chambarel, C. Kharif, and J. Touboul. Head-on collision of two solitary waves and residual falling jet formation. *Nonlin. Processes Geophys.*, 16:111–122, 2009. [5](#)
- [7] F. Chazel, D. Lannes, and F. Marche. Numerical simulation of strongly nonlinear and dispersive waves using a Green-Naghdi model. *J. Sci. Comput.*, 48:105–116, 2011. [2](#)
- [8] D. Clamond and D. Dutykh. Practical use of variational principles for modeling water waves. *Physica D: Nonlinear Phenomena*, 241(1):25–36, 2012. [2](#)
- [9] D. Clamond, M. Francius, J. Grue, and C. Kharif. Long time interaction of envelope solitons and freak wave formations. *Eur. J. Mech. B/Fluids*, 25(5):536–553, 2006. [2](#)
- [10] M. J. Cooker, P. D. Weidman, and D. S. Bale. Reflection of a high-amplitude solitary wave at a vertical wall. *J. Fluid Mech.*, 342:141–158, 1997. [5](#)
- [11] W. Craig, P. Guyenne, J. Hammack, D. Henderson, and C. Sulem. Solitary water wave interactions. *Phys. Fluids*, 18(5):57106, 2006. [3](#), [4](#)
- [12] F. Dias and P. Milewski. On the fully-nonlinear shallow-water generalized Serre equations. *Physics Letters A*, 374(8):1049–1053, 2010. [2](#)
- [13] D. Dommermuth. The initialization of nonlinear waves using an adjustment scheme. *Wave Motion*, 32(4):307–317, Oct. 2000. [5](#)
- [14] D. Dutykh, D. Clamond, P. Milewski, and D. Mitsotakis. Finite volume and pseudo-spectral schemes for the fully nonlinear 1D Serre equations. *Accepted to European Journal of Applied Mathematics*, pages 1–27, 2013. [2](#), [4](#), [5](#)
- [15] G. A. El, R. H. J. Grimshaw, and N. F. Smyth. Unsteady undular bores in fully nonlinear shallow-water theory. *Phys. Fluids*, 18:27104, 2006. [5](#)
- [16] J. D. Fenton and M. M. Rienecker. A Fourier method for solving nonlinear water-wave problems: application to solitary-wave interactions. *J. Fluid Mech.*, 118:411–443, Apr. 1982. [3](#), [4](#)
- [17] Y. Goda. *Random Seas and Design of Maritime Structures*, volume 33 of *Advanced Series on Ocean Engineering*. World Scientific, 2010. [1](#)
- [18] A. E. Green, N. Laws, and P. M. Naghdi. On the theory of water waves. *Proc. R. Soc. Lond. A*, 338:43–55, 1974. [2](#)
- [19] A. E. Green and P. M. Naghdi. A derivation of equations for wave propagation in water of variable depth. *J. Fluid Mech.*, 78:237–246, 1976. [2](#)
- [20] J. Hammack, D. Henderson, P. Guyenne, and M. Yi. Solitary wave collisions. In *Proc. 23rd International Conference on Offshore Mechanics and Arctic Engineering*, 2004. [4](#)

- [21] J. D. Hansom and A. M. Hall. Magnitude and frequency of extra-tropical North Atlantic cyclones: A chronology from cliff-top storm deposits. *Quaternary International*, 195:42–52, 2009. [10](#)
- [22] D. Kelletat. Comments to Dawson, A.G. and Stewart, I. (2007), Tsunami deposits in the geological record.-Sedimentary Geology 200, 166-183. *Sedimentary Geology*, 211:87–91, 2008. [10](#)
- [23] D. Lannes and P. Bonneton. Derivation of asymptotic two-dimensional time-dependent equations for surface water wave propagation. *Phys. Fluids*, 21:16601, 2009. [2](#)
- [24] Y. A. Li. Hamiltonian structure and linear stability of solitary waves of the Green-Naghdi equations. *J. Nonlin. Math. Phys.*, 9(1):99–105, 2002. [2](#)
- [25] C. M. Linton and P. McIver. *Mathematical Techniques for Wave/Structure Interactions*. Chapman & Hall/CRC, 2001. [2](#)
- [26] T. Maxworthy. Experiments on collisions between solitary waves. *J Fluid Mech*, 76:177–185, 1976. [4](#)
- [27] C. C. Mei. *The applied dynamics of water waves*. World Scientific, 1989. [4](#)
- [28] N. R. Mirchina and E. Pelinovsky. Increase in the amplitude of a long wave near a vertical wall. *Izvestiya, Atmospheric and Oceanic Physics*, 20(3):252–253, 1984. [4](#)
- [29] I. Nikolkina and I. Didenkulova. Rogue waves in 2006 - 2010. *Nat. Hazards Earth Syst. Sci.*, 11:2913–2924, 2011. [2](#)
- [30] L. O’Brien, J. M. Dudley, and F. Dias. Extreme wave events in Ireland: 14 680 BP-2012. *Natural Hazards and Earth System Science*, 13(3):625–648, Mar. 2013. [2](#), [10](#)
- [31] E. N. Pelinovsky, E. Troshina, V. Golinko, N. Osipenko, and N. Petrukhin. Runup of tsunami waves on a vertical wall in a basin of complex topography. *Phys. Chem. Earth. (B)*, 24(5):431–436, 1999. [5](#)
- [32] M. Sainflou. Essai sur les digues maritimes verticales. *Annales des Ponts et Chaussées*, 98(11):5–48, 1928. [1](#)
- [33] A. Scheffers, D. Kelletat, S. Haslett, S. Scheffers, and T. Browne. Coastal boulder deposits in Galway Bay and the Aran Islands, western Ireland. *Zeitschrift für Geomorphologie*, 54(3):247–279, 2010. [10](#)
- [34] A. Scheffers, S. Scheffers, D. Kelletat, and T. Browne. Wave-Emplaced Coarse Debris and Megaclasts in Ireland and Scotland: Boulder Transport in a High-Energy Littoral Environment. *Journal of Geology*, 117(5):553–573, 2009. [10](#)
- [35] F. Serre. Contribution à l’étude des écoulements permanents et variables dans les canaux. *La Houille blanche*, 8:374–388, 1953. [2](#)
- [36] L. F. Shampine. ODE solvers and the method of lines. *Numerical Methods for Partial Differential Equations*, 10(6):739–755, 1994. [4](#)
- [37] L. F. Shampine and M. W. Reichelt. The MATLAB ODE Suite. *SIAM Journal on Scientific Computing*, 18:1–22, 1997. [4](#)
- [38] J. J. Stoker. *Water Waves: The mathematical theory with applications*. Interscience, New York, 1957. [2](#)
- [39] C. H. Su and R. M. Mirie. On head-on collisions between two solitary waves. *J. Fluid Mech.*, 98:509–525, 1980. [4](#)
- [40] M. Tissier, P. Bonneton, F. Marche, F. Chazel, and D. Lannes. Nearshore Dynamics of Tsunami-like Undular Bores using a Fully Nonlinear Boussinesq Model. *Journal of Coastal Research*, 64:603–607, 2011. [2](#), [5](#)
- [41] G. Wei, J. T. Kirby, S. T. Grilli, and R. Subramanya. A fully nonlinear Boussinesq model for surface waves. Part 1. Highly nonlinear unsteady waves. *J. Fluid Mech.*, 294:71–92, 1995. [2](#), [5](#)
- [42] D. M. Williams. Mechanisms of wave transport of megaclasts on elevated cliff-top platforms: examples from western Ireland relevant to the storm-wave versus tsunami controversy. *Irish Journal of Earth Sciences*, 28:13–23, 2010. [10](#)
- [43] N. J. Zabusky and M. D. Kruskal. Interaction of solitons in a collisionless plasma and the recurrence of initial states. *Phys. Rev. Lett.*, 15:240–243, 1965. [3](#)
- [44] M. I. Zheleznyak and E. N. Pelinovsky. Physical and mathematical models of the tsunami climbing a beach. In E. N. Pelinovsky, editor, *Tsunami Climbing a Beach*, pages 8–34. Applied Physics Institute Press, Gorky, 1985. [2](#)

UNIVERSITY COLLEGE DUBLIN, SCHOOL OF MATHEMATICAL SCIENCES, BELFIELD, DUBLIN 4, IRELAND

E-mail address: `Francesco.Carbone@ucd.ie`

UNIVERSITY COLLEGE DUBLIN, SCHOOL OF MATHEMATICAL SCIENCES, BELFIELD, DUBLIN 4, IRELAND AND LAMA, UMR 5127 CNRS, UNIVERSITÉ DE SAVOIE, CAMPUS SCIENTIFIQUE, 73376 LE BOURGET-DU-LAC CEDEX, FRANCE

E-mail address: `Denys.Dutykh@ucd.ie`

URL: <http://www.denys-dutykh.com/>

DÉPARTEMENT D'OPTIQUE P.M. DUFFIEUX, UNIVERSITÉ DE FRANCHE-COMTÉ, INSTITUT FEMTO-ST CNRS UMS 6174, BESANÇON, FRANCE

E-mail address: `John.Dudley@univ-fcomte.fr`

CMLA, ENS CACHAN, CNRS, 61 AVENUE DU PRÉSIDENT WILSON, F-94230 CACHAN, FRANCE AND UNIVERSITY COLLEGE DUBLIN, SCHOOL OF MATHEMATICAL SCIENCES, BELFIELD, DUBLIN 4, IRELAND

E-mail address: `Frederic.Dias@ucd.ie`